Electron vacancy-level dependent hybrid photoionization of the F⁻@C₆₀⁺ molecule: a novel effect

Esam Ali¹, Taylor O'Brien¹, Andrew Dennis¹, Mohamed El-Amine Madjet^{1,2}, Steven T Manson³ and Himadri S Chakraborty^{1,*}

- Department of Natural Sciences, D.L. Hubbard Center for Innovation, Northwest Missouri State University, Maryville, Missouri 64468, United States of America
- Max-Planck-Institut f
 ür Physik Komplexer Systeme, N
 öthnitzer Stra
 ße 38, 01187 Dresden, Germany
- ³ Department of Physics and Astronomy, Georgia State University, Atlanta, Georgia 30303, United States of America

E-mail: eaagx2@mst.edu and himadri@nwmissouri.edu

Received 12 October 2021, revised 12 January 2022 Accepted for publication 28 January 2022 Published 28 February 2022



Abstract

Our previous studies (Shields *et al* 2020 *J. Phys.* B: At. Mol. Opt. Phys. **53** 125101; Shields *et al* 2020 *Euro. Phys. J. D* **74** 191) have predicted that the atom-fullerene hybrid photoionization properties for X = Cl, Br and I endohedrally confined in C_{60} are different before and after an electron transfers from C_{60} to the halogen. It was further found as a rule that the ionization dynamics is insensitive to the C_{60} level the electron originates from to produce $X^- @ C_{60}^+$. In the current study, we report an exception to this rule in $F @ C_{60}$. It is found that when the electron vacancy is situated in the C_{60} level that participates in the hybridization in $F^- @ C_{60}^+$, the mixing becomes dramatically large leading to strong modifications in the photoionization of the hybrid levels. This novel effect is fundamentally based on a level-crossing phenomenon driven by the electron transfer in $F @ C_{60}$. But when the vacancy is at any other pure level of C_{60} , the level-invariance is retained showing weak hybridization. Even though this case of $F @ C_{60}$ is an exception in the halogen $@ C_{60}$ series, the phenomenon can be more general and can occur with compounds of other atoms caged in a variety of fullerenes. Possible experimental studies are suggested to benchmark the present results.

Keywords: photoionizations, hybridization, endofullerenes, level-crossing, DFT, electron-transfer

(Some figures may appear in colour only in the online journal)

1. Introduction

Progress in synthesis and isolation techniques [1] of endohedral fullerenes, an atom taken hostage in a fullerene cavity, or endofullerenes for short, present opportunities for their experimental and motivations for their theoretical studies. One attraction for such studies arises from the interesting symmetry and

great stability of these systems of natural molecular traps. The other is the fact that a vast range of existing and potential technologies, encompassing photovoltaics [2], superconductivity [3], quantum computations [4, 5], molecular device [6] and bio-medics [7], uses materials that have endofullerenes at their core. Such technologies and their further developments may find underpinnings of success from the information obtained via fundamental spectroscopic studies of these molecules.

In order to study the ionizing response of vapor-phase endofullerenes to UV electromagnetic radiations, a series of

^{*} Author to whom any correspondence should be addressed.

measurements [8–10] was conducted using merged beam techniques at the Berkeley Advanced Light Source. With the increase of sample production rates, there are future possibilities of performing photoelectron spectroscopic experiments [11] on these systems. A swath of theoretical studies at various levels of approximation on the photoionization of endofullerenes with closed shell atoms also exists [12, 13]. In particular, hybridization of high-lying orbitals of the central atom with C_{60} and explorations of the photoionization properties of these hybrid levels have regularly been predicted [14–18]. Hybrid levels are unique, for they expose interference features from the atom-fullerene coherent ionization which are absent in the isolated systems.

Endofullerenes of open-shell atoms, on the other hand, may also have interesting applied relevance [19]. At a rather exotic level, $N@C_{60}$ exhibited uniquely long spin relaxation times driven by the confinement [20], $P@C_{60}$ displayed an enhancement in hyperfine coupling of the phosphorous' unpaired electrons with its nucleus [21], and muonium@ C_{60} indicated a diminution of the hyperfine interaction between the positively-charged muon and the unpaired electrons [22].

Computations of nonlinear optical response were done on endofullerene dimers where F@C₆₀ is used as one monomer [23]. A recent calculation [24] revealed a whole electron transfer from C₆₀ to the molecular F₂, despite C₆₀'s high electron affinity, forming $F_2^-@C_{60}^+$. Very recently, we performed theoretical photoionization studies of isolated halogen endofullerenes $Cl@C_{60}$ [25], $Br@C_{60}$ and $I@C_{60}$ [26]. A halogen atom with an outer-shell electron vacancy (hole) can be reactive and can readily capture an electron from C₆₀ to acquire a stable configuration. However, this transfer will need energy, since the electron affinity level energies of halogens are higher than the binding energy of C_{60} HOMO level. Of course, there will be extra binding due to the electrostatic attraction between F⁻ and C₆₀⁺. However, some such stable configurations with the electron coming from deeper C₆₀ levels may actually be metastable due to the need for larger transition energies. In any case, the realistic ground state of the compound may be a mixture of configurations, before and after the electron transfer. Therefore, knowledge of photoionization properties of all molecular states can be useful to reveal the actual configuration of the molecule by photoelectron spectroscopic experiments. Furthermore, multiple metastable states are known to form in other processes, such as, in slow electron collisions leading to the formation of negative ions of fullerene molecules [27]. Therefore, a knowledge repository of endofullerenes with various stable and metastable electronic structures accessed by photoionizating the atom-fullerene hybrid levels can have cross-topical relevance as well.

2. Novel effects of level-crossings

There may arise a new phenomenon originating from the neardegeneracy due to energy-crossing between an atomic and a fullerene level driven by the electron transfer. Fundamental effects generated by level-crossing are abound. A simple example is the transition metals in the periodic table: up to Ca, the 3d level is an excited state being above 4s. But by Sc, 3d moves into the ground state by crossing 4s and the ground state photoionization cross section of Sc changes dramatically from Ca. Another example is the near-threshold dramatic photoionization behavior of Si⁴⁺ in the Ne isoelectronic sequence [28]. This happens as the inner $2s \rightarrow 3p$ excited (autoionizing) state crosses the $2s^{22}p^{52}P_{1/2}$ ionization threshold along the sequence such that the resulting resonance just straddles the ionization limit at Si⁴⁺. A maximum entanglement between nuclear and electron spins is predicted for atoms at avoided crossings demonstrating a relation between the level crossings and Berry phases at the level of the Breit-Rabi Hamiltonian [29]. Recently, the effect of chirped laser-pulse control in the interference between different pathways to study the momentum-dependent wave-packet using molecular levelcrossing spectroscopy is studied [30]. Experimentally, a very efficient transfer through molecular bound states is shown by magnetically tuned mixing of two neighboring molecular levels [31]; this activated forbidden radio-transitions. Hence, exploring effects of atom-fullerene level-crossing on absorption properties as a function of spectral charge distribution can unfurl new horizon of studies in endofullerene materials. In other words, new phenomena can arise from level-crossings; in particular, from the near-degeneracy due to a level-crossing between an atomic and a fullerene level driven by the electron transfer.

It was found in our previous studies [25, 26] that the photoionization properties of the configurations of $\mathrm{Cl^-@C_{60}}^+$, $\mathrm{Br^-@C_{60}}^+$ and $\mathrm{I^-@C_{60}}^+$ were not sensitive to the particular $\mathrm{C_{60}}$ level where the hole is located. This is because, as shown in figure 1, the valence np levels of the isolated $X = \mathrm{Cl}$, Br , and I are energetically above the 2p level of empty $\mathrm{C_{60}}$ (in the jellium model) that participates in the hybridization. When an electron in $X@\mathrm{C_{60}}$ is captured by the central atom, the resulting screening effect shifts the atomic np level even higher. So the separation of interacting levels gets so large that it becomes irrelevant whether the electron that moved was a pure $\mathrm{C_{60}}$ electron or a hybrid electron of $X@\mathrm{C_{60}}$. Thus, the modification of the hybridization after the transfer becomes effectively insensitive to the vacancy level of $X^-\mathrm{@C_{60}}^+$.

The situation, however, is very different if the free atomic level locates, on the other hand, below $2pC_{60}$ as is the case for the smallest halogen F (see figure 1). In forming F⁻@C₆₀⁺, the screening from the electron transfer will cause 2pF to rise and move toward 2pC₆₀ from below it (figure 1, bottom left panel). This will create the condition of a reduced level separation, instead of the increase as happens for other halogens. The effect may sensitize the hybridization mechanism. For example, the transfer of a hybrid versus a pure C₆₀ electron could make a difference. These transfers are illustrated in figure 1, which also displays the resulting hybrid energy-levels and radial wavefunctions, respectively, in the middle and the right bottom panels. As we demonstrate in this paper, the hybridization indeed becomes dramatically higher when the vacancy is generated in the hybrid-active level of F@C₆₀ (bottom middle panel). To illustrate the effect of the vacancy at a pure (hybrid-passive) level which greatly minimizes the hybridization, HOMO C₆₀ is considered (bottom

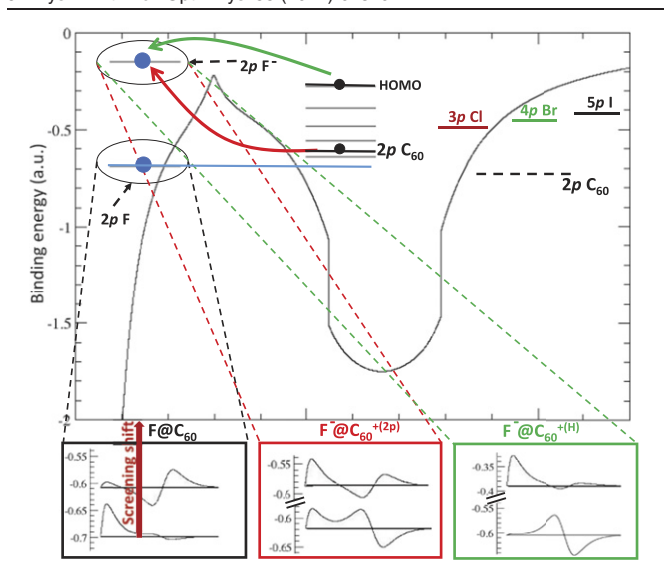


Figure 1. A schematic that illustrates the C_{60} vacancy-level dependence in the ground state hybridization of the compound (see text).

right panel), since the result is found practically identical for any pure C_{60} vacancy. Strong implications of this phenomenon on the hybrid level photoionization of $F^-@{C_{60}}^+$, a hitherto unknown effect, will be presented by comparing cross sections calculated with the hole in different ${C_{60}}^+$ levels.

3. Theoretical model in brief

The details of the theoretical schemes are described in reference [15] and more recently in reference [25]. Choosing the photon polarization along the *z*-axis, the photoionization dipole transition cross section in a linear response approximation of time-dependent density-functional theory (DFT) is given by,

$$\sigma_{n\ell \to k\ell'} \sim |\langle \psi_{\mathbf{k}\ell'} | z + \delta V | \phi_{n\ell} \rangle|^2.$$
 (1)

Here **k** is the momentum of the continuum electron, z is the one-body dipole operator, ϕ_{nl} is the single electron bound wavefunction of the target level, and $\psi_{\mathbf{k}l'}$ is the respective outgoing dipole-allowed continuum wavefunction, with $l'=l\pm 1$. δV represents the complex induced potential that accounts for electron correlations within the linear response of the electrons to the photon field. The computation of δV involves determining photon energy dependent induced change in the electron density to be obtained by varying the ground state potential with respect to the ground state electron density as described in reference [32].

We model the bound and continuum states, and the ground state potential, using the independent particle DFT approximation that utilizes the Leeuwen–Baerends (LB) exchange-correlation functional [33]. This functional involves the gradient of the electron density in the scheme described earlier [34]. We chose the spherical frame with F or F⁻ situated at the center of C₆₀. The polarization interaction of F⁻ may induce some offset in its position from the center. However, a

DFT simulation with Born–Oppenheimer molecular dynamics found F^- oscillation within neutral C_{60} to be rather small [35] and a relatively weak effect on the photoionization process from such small offset was predicted [36]. Earlier studies also showed small effects of the cage polarization except very close to the ionization threshold [37].

A core of 60 C⁴⁺ ions for C₆₀ is constructed by smearing the total positive charge over a spherical jellium shell with known molecular radius R = 6.70 a.u. (3.54\AA) [11] and thickness Δ . The Kohn-Sham equations for the system of 240 C_{60} electrons (four valence $2s^22p^2$ electrons from each carbon atom), plus all electrons of the central atom/ion, are then solved self-consistently. The values of Δ and a pseudo potential used are determined both by requiring charge neutrality and obtaining the experimental value [38] of the first ionization threshold of C_{60} . $\Delta = 2.46$ a.u. (1.30 Å) thus obtained closely agree with the value extracted from measurements [11, 39]. Within this framework, we also selectively omit either F (F⁻) or C_{60} (C_{60} ⁺) to obtain the corresponding empty C_{60} (C_{60}^+) and free F (F⁻) results. Parametric optimization of LB functional followed the scheme utilized in the previous work [26] to reproduce the values of the ionization potential and the electron affinity of F from the NIST database within 20%.

4. Results and discussion

4.1. Ground state hybridization versus vacancy levels

In an endofullerene system, an eigenstate of the free atom can only couple with an eigenstate of the empty C_{60} of the same angular momentum symmetry (due to the orthogonality of spherical wavefunctions) to produce a pair of hybrid eigenstates of the composite system. For F@C₆₀ this occurs between valence 2pF and 2pC₆₀ states to produce symmetric and antisymmetric hybrid states of F@C₆₀ as,

$$|\mathbf{F} \pm \mathbf{C}_{60}\rangle = \eta_{\pm} |\phi_{2p\,\mathbf{F}}\rangle \pm \eta_{\mp} |\phi_{2p\,\mathbf{C}_{60}}\rangle \tag{2}$$

for $F@C_{60}$, and the same for $F^-@C_{60}^+$ with F and C_{60} replaced by F⁻ and C₆₀⁺. Here $\eta_+ = \sqrt{\alpha}$ and $\eta_- = \sqrt{1-\alpha}$, where α is the mixing parameter that renders the hybrid states orthonormal. We use the hydrogenic Coulomb notation of labeling for F and F $^-$, such that the corresponding 2p wavefunctions are radially nodeless. The standard harmonic oscillator notion is used for C_{60} and C_{60}^+ where their 2p wavefunctions have one radial node. The radial component of these hybrid wavefunctions are, respectively, shown in figures 2(a) and (b). In general, the hybridization is favored when the energy separation between the reacting levels decreases and their wavefunction overlap increases; these energies and wavefunctions are also shown in figure 2. While the free 2p F level is just below empty $2pC_{60}$, their wavefunction overlap is small owing to the small size of F leading to a weak hybridization in F@C₆₀. As seen, the deeper symmetric hybrid $F + C_{60}$ [figure 2(a)] still retains significant F character, while the weaker-bound antisymmetric hybrid $F - C_{60}$ [figure 2(b)] continues to remain largely C₆₀-like. On the other hand, the hybrid states of $F^-@C_{60}^{+(H)}$ with the vacancy at the HOMO

-21.8

10

12

C₆₀ level (which does not participate in hybridization), also plotted in figure 2, present the opposite picture: the significantly weaker bound antisymmetric hybrid [figure 2(b)] now becomes F⁻-type, while the symmetric hybrid [figure 2(a)] is of C₆₀-type. We find practically the same degree of mixing when the vacancy is at any other hybrid-passive C_{60} level, like HOMO, that remains pure in the compound. Note the following in going from F@C $_{60}$ to F^-@C $_{60}^{+(\,H)}$ in figure 2: (i) the binding energy of the F⁻-dominant hybrid level is significantly lower than that of the F-dominant hybrid level which is because of the stronger screening of the F nucleus due to the extra electron that was transferred to the atomic zone. However, (ii) the cage-dominant hybrids remain energetically close primarily due to the fact that the relocation of a single electron hardly affects the screening of the cage states owing to the large electron population of C₆₀. In effect, therefore, the F-dominated level swings past the almost stagnant cage-dominated level as the molecular configuration switches from $F@C_{60}$ to $F^-@C_{60}^{+(H)}$. However, if we choose the configuration $F^-@C_{60}^{+(2p)}$, that is the vacancy in the hybridactive $2pC_{60}$ level, the hybridization becomes very strong with the hybrid level energies being very close, as figure 2 further displays. For a quantitative estimate of this effect, we fit equation (2) to the hybrid wavefunctions of $F^-@C_{60}^{+(2p)}$ to obtain $\alpha = 0.2925$, resulting in $\eta_+ = 0.541$ and $\eta_- = 0.841$; the fitted curves are included in figure 2. The bottom three panels of figure 1 together summarize the essence of the total phenomenon.

To understand the underlying physics that leads to the enhancement of the hybridization in $F^-@C_{60}^+$ when the vacancy is in $2pC_{60}$ versus in HOMO C_{60} , we use a qualitative picture. Although the calculation is done by placing a F⁻ ion in a C_{60}^+ cage directly, it is convenient to consider a two step model. First consider the ground state of F@C₆₀. Then we use the levels of F@C₆₀, including its hybrid levels, as the basis to analyze the hybridization after an electron moves from C₆₀ to F. This electron transfer is considered selectively from two levels: (i) from HOMO of F@C60 which is also HOMO of C_{60} and a pure C_{60} level and (ii) from $F-C_{60}$ which is a hybrid level of F@C₆₀ but of dominantly cage-type and energetically shallower than the other hybrid $F + C_{60}$ which is dominantly F-type (figure 2). In the first case it is a 'whole' electron that transfers to the F-zone and causes a 'complete' screening of the atomic nucleus. This causes the F-dominant hybrid of F@C₆₀ to energetically shift upward, cross the practically unmoved cage-dominant hybrid and move far above to result in yet another weak hybridization in $F^-@C_{60}^{+(H)}$, albeit a symmetry reversal as noted above and seen in figure 2. This effect will be quite general as long as the transferring electron originates from any of the pure C_{60} states of F@ C_{60} , even though the total energy of resulting configurations will be different in each case. However, when the electron comes from the hybrid $F - C_{60}$ level, effectively a 'partial' electron transfers, inducing a rather 'incomplete' screening effect. Consequently, the F-dominant level will still up-shift, but under a weaker screening will not be able to separate far enough from the C₆₀-dominated hybrid level. This, along with the fact

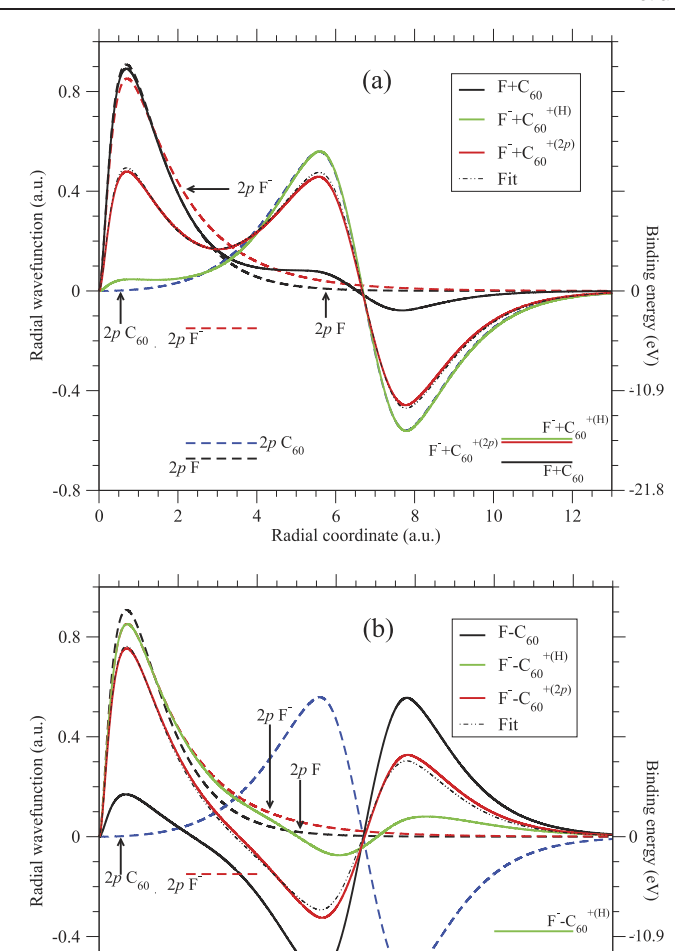


Figure 2. Radial wavefunctions (left vertical scale) and level energies (right vertical scale) of the symmetric (a) and antisymmetric (b) hybrid states of $F@C_{60}$, $F^-@C_{60}^{+(H)}$, and $F^-@C_{60}^{+(2p)}$ are displayed. The curves by fitting equation (2) to $F^-@C_{60}^{+(2p)}$ wavefunctions are given. Wavefunctions and energies of 2pF (F^-) and $2pC_{60}$ are also shown for reference.

Radial coordinate (a.u.)

that the overlap between $F - C_{60}$ and $F + C_{60}$ wavefunctions is large due to their non-vanishing amplitudes on both F and C_{60} regions, will favor their increased mixing in the resulting configuration of $F^-@{C_{60}}^{+(2p)}$. Thus, the electron-transfer induced near-degeneracy as a 'novel tipping-point' accentuates the atom-fullerene hybrid emission as shown in the following.

It is true that the relatively weak hybridization in $F@C_{60}$ does not, as such, suggest too strong a reduction of screening to support a small enough up-shift of the F-dominant level so that the effect justifies the strong enhancement of hybridization as seen in $F^-@C_{60}^{+(2p)}$. But we argue that this is a limitation of the two-step model we use here to visualize the basic effect qualitatively, but not to quantify it. The real mechanism is a one-step adiabatic process where a F^- anion is so rapidly formed that it does not allow the states of $F@C_{60}$ to relax enough. In effect, in the real system, the mixing and

the transfer happen simultaneously between the same levels that hybridize. This feature is also borne out in our observation that equation (2), that includes wavefunctions of neutral F and C_{60} , provides a somewhat better fit (figure 2) to $F^- @C_{60}^{+(2p)}$ hybrids than using wavefunctions of ionic systems in equation (2). As pointed out, in the F atom, unlike other halogens, the valence 2p level has a higher binding energy than $2pC_{60}$, and that is the key here. This is so that with smaller screening in $F^- @C_{60}^{+(2p)}$ the participant levels can still stay within a narrow energy proximity to strongly hybridize, while for $F^- @C_{60}^{+(H)}$ with full screening the levels cross but then separate out far enough to retain the weak hybridization. In contradistinction, the np levels of Cl, Br and I being less bound than $2pC_{60}$ to begin with forbid this effect.

We note that previous structure calculations indeed predicted partial electron transfer from C₆₀ to F in F@C₆₀ with net charge on F to be -0.29 [40]. This study asserted no possibility of reverse transfer from F to C_{60} and indicated ionization signals from hybridized 2pF orbitals. Separately, we have also computed the partial charge on F in the compound by using the density-derived electrostatic and chemical scheme [41] to find the charge of the F atom to be a fractional -0.43. The method was based on calculating the ground state partial charge distribution of F@C₆₀ using the PBE exchange-correlation functional. The result likely corroborates our assertion in the Introduction that the real ground state may be a mixture of configurations, before and after the electron transfer. The HOMO electron showing a tendency to move to the F site already at the ground state also favors the likelihood to undergo a complete transfer upon excitation.

4.2. Hybrid photoionization versus vacancy levels

Cross sections calculated in linear response timedependent DFT for three systems $F@C_{60}$, $F^-@C_{60}^{+(H)}$, and $F^{-} @C_{60}^{+(2p)}$ are presented in figure 3 with panel (a) and (b), respectively, for emissions from the symmetric and the antisymmetric levels. It is seen that the lower-energy portions of all of the endofullerenes are fraught with narrow resonances, primarily related to C₆₀ and are not there for free atoms (shown). The resonances result both from inner-shell single-electron excitation Auger and inter-Coulombic decay processes [42]. Included in these cluster of resonances are the Auger-ICD hybridized decay processes as well [18]. In addition, note that the symmetric $F + C_{60}$ and antisymmetric $F-C_{60}$ level cross sections closely match, respectively, the antisymmetric $F^--{C_{60}}^{+(\,H)}$ and symmetric $F^-+{C_{60}}^{+(\,H)}$ level cross sections. This is expected because their corresponding radial wavefunctions simply transpose the symmetry while exhibiting largely the same composition of mixing, as discussed in the previous subsection. The one noticeable difference is that the $F^- - C_{60}^{+(H)}$ cross section, due to this level's lower binding, opens at much lower photon energy than that of $F + C_{60}$.

4.2.1. Low energy spectra. Comparing all the hybrid level results with the 2p cross sections of free F and F⁻, which practically overlap with each other, and with 2p of empty C_{60} indicates plasmon driven enhancements and structures at

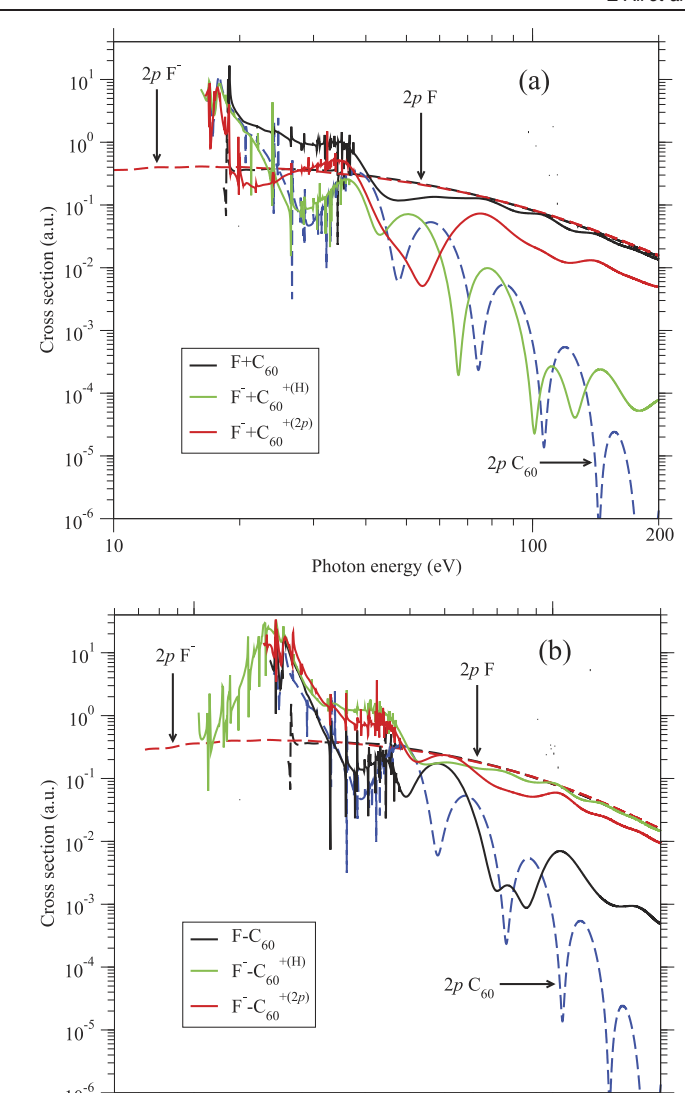


Figure 3. Photoionization cross sections of the symmetric (a) and antisymmetric (b) hybrid levels of $F@C_{60}$, $F^-@C_{60}^{+(H)}$, and $F^-@C_{60}^{+(2p)}$. Cross sections of 2pF (F^-) and $2pC_{60}$ are also presented.

Photon energy (eV)

10

lower photon energies [14, 17, 18, 43]. In the framework of interchannel coupling (IC) due to Fano [44], the correlation-modified matrix element of the photoionization of $X \pm C_{60}$ can be written perturbatively as [17, 25, 26],

$$\mathcal{M}_{\pm}(E) = \mathcal{D}_{\pm}(E) + \sum_{n\ell} \int dE' \frac{\langle \psi_{n\ell}(E') | \frac{1}{|\mathbf{r}_{\pm} - \mathbf{r}_{n\ell}|} | \psi_{\pm}(E) \rangle}{E - E'} \times \mathcal{D}_{n\ell}(E')$$
(3)

in which the single electron (uncorrelated) matrix element, that is the matrix element without δV in equation (1), is

$$\mathcal{D}_{\pm}(E) = \langle ks(d)|z|\phi_{\pm}\rangle \tag{4}$$

100

and $|\psi_{nl}\rangle$ in the IC integral is the (continuum) wavefunction of the $n\ell \to k\ell'$ channel. Taking the hybridization into account,

the channel wavefunctions in equation (6) become

$$|\psi_{\pm}\rangle = \eta_{\pm}|\psi_{2pX}\rangle \pm \eta_{\mp}|\psi_{2pC_{60}}\rangle. \tag{5}$$

Substituting equation (5) into equation (6), and noting that the overlap between a pure X (X^-) bound state and a pure C_{60} (C_{60}^+) bound state is negligible, since they occupy different regions of space, we separate the atomic and fullerene contributions to the integral to get the full (correlated) matrix element for $X \pm C_{60}$ and $X^- \pm C_{60}^+$ levels as,

$$\mathcal{M}_{\pm}(E) = \eta_{\pm} \mathcal{M}_{2pX(X^{-})}(E) \pm \eta_{\mp} \mathcal{M}_{2pC_{60}(C_{60}^{+})}(E),$$
 (6)

where the first and second terms, respectively, on the right-hand side describes IC effects of atomic and fullerene ionization channels. Note that $\mathcal{M}_{2pX(X^-)}$ and $\mathcal{M}_{2pC_{60}(C_{60}^+)}$ are the IC matrix elements constructed via coupling respectively among *pure* atomic and fullerene channels.

Dominant fullerene characters of $F^- + C_{60}^{+(H)}$ and F -C₆₀ wavefunctions (figure 2) ensure dominant fullerene IC effects in equation (6). This explains why the corresponding cross sections at lower energies almost follow the empty $2p C_{60}$ result in figure 3. For $F^- - C_{60}^{+(H)}$ and $F + C_{60}$ cross sections, on the other hand, while their dominant atomic character brings them close to the free $2pF(F^-)$ results at higher energies, their enhancements at lower energies are notable. This enhancement is due to an IC driven mechanism discussed previously [43] that siphons off giant-size strengths from the fullerene plasmonic emission even though the fullerene admixture of these hybrid wavefunctions is quite small. However, note a rather dramatic difference between the symmetric F⁻ + $C_{60}^{+(2p)}$ and $F^- + C_{60}^{+(H)}$ results in figure 3(a) over, in fact, the entire energy range shown. This owes to the increased hybridization process in the $F^- + C_{60}^{+(2p)}$ discussed above as the main finding of this study. The process subsequently yields comparable atomic and fullerene IC effects in equation (6) including a comparable contribution of their coherence. On the other hand, there is not-so-dramatic differences between antisymmetric F^- – ${C_{60}}^{+(2\it{p})}$ and F^- – ${C_{60}}^{+(\rm{\,H})}$ results in figure 3(b). In sum, we find a most interesting and unexpected phenomenology; the symmetric case, figure 3(a), is very strongly dependent upon the location of the C₆₀ vacancy, but the antisymmetric case is not. This must mean that there are cancellations in the matrix elements in the antisymmetric case that are not present for the symmetric

4.2.2. Higher energy spectra. As the plasmonic effect weakens with increasing energy, oscillatory modulations at varied degrees of prominence show up in the cross sections. These oscillations are a consequence of a well-known interference mechanism [45] due to the cavity structure of C_{60} which was modeled earlier in detail in reference [46]. At such high energies the IC in equation (6) is no longer important, but the hybridization remains, so that equation (6) simplify to

$$\mathcal{D}_{\pm}(E) = \eta_{\pm} \mathcal{D}_{2pX(X^{-})}(E) \pm \eta_{\mp} \mathcal{D}_{2pC_{60}(C_{co}^{+})}(E). \tag{7}$$

The interference model is based on the following mechanism. The matrix element \mathcal{D}_{\pm} can generally be separated into two

components, one arising from the atomic region and other from the C_{60} shell region, and can be written down, respectively, as follows [46]

$$\mathcal{D}_X \sim \mathcal{D}^{\text{atom}}(k) + A^{\text{refl}}(k) \left[e^{-ikD_0} e^{-iV_0 \frac{2\Delta}{k}} - e^{-ikD_i} \right]$$
 (8a)

$$\mathcal{D}_{C} \sim A^{\text{shell}}(k) e^{-i\frac{V_{0}}{k}} \left[a_{i} e^{-ikR_{i}} - a_{o} e^{-ikR_{o}} \right],$$
 (8b)

where the photoelectron momentum $k=\sqrt{2(E-\epsilon_\pm)}$ in atomic units, $a_{\rm i}$ and $a_{\rm o}$ are the values of ϕ_\pm at the inner and outer radii $R_{\rm i}$ and $R_{\rm o}$ of C_{60} , and V_0 is the average depth of the shell potential. In equation (8a) $\mathcal{D}^{\rm atom}$ represents the direct ionization amplitude from the atomic region. The second term in this equation embodies the reflection of this outgoing photoelectron wave from both inner and outer surfaces of the shell. Quantitatively, this induces oscillations as a function of the photoelectron momentum with amplitude $A^{\rm refl}$ and frequencies related to $D_{\rm i}$ and $D_{\rm o}$, the inner and outer diameters of the shell. The direct and the reflected parts coherently interfere in the cross section.

Since A^{refl} is proportional to $\mathcal{D}^{\text{atom}}$, the larger the atomic component of a hybrid wavefunction, the stronger is the reflection and the higher is the chances that the oscillations occur about the free atom (ion) result. This is exactly what is seen for the high energy cross section of the F-dominant levels of F@C $_{60}$ and F $^-$ @C $_{60}^{+(\,{\rm H})}$ that follow the $2p{\rm F}$ result in figure 3. On the other hand, equation (8b), resulting from the overlap integral in the shell region, produces two localized emissions in the vincities of the shell edges, where the available ionizing forces maximize due to rapid variations of the shell potential there. Such a diffraction-type effect translates into another oscillation in frequencies related to R_i and R_o . This part will also add to the coherent interference in the cross section and will dominate if a hybrid level has a stronger C₆₀ character, like for the C₆₀-dominant levels of F@C₆₀ and $F^-@C_{60}^{+(H)}$ in figure 3. Indeed, the oscillation structures in the cross section of these hybrid levels intensify at higher energies while the average value fall lower than free 2p F as exhibited in figure 3.

As already noted above, for the $F^- @C_{60}^{+(2p)}$ hybrids, due to their almost comparable share of atom- C_{60} character, the differences in the corresponding cross section shapes arise from the interference among strong direct atomic, reflective and relatively comparable diffractive emissions. As pointed out above, the particularly strong differences between the high-energy results of symmetric $F^- + C_{60}^{+(2p)}$ and $F^- + C_{60}^{+(H)}$ and relatively weaker differences between antisymmetric $F^- - C_{60}^{+(2p)}$ and $F^- - C_{60}^{+(H)}$ are noted in figure 3. These differences further identify the importance of hybrid versus pure vacancies in $F^- @C_{60}^+$ in the spectroscopic details of higher energy emission structure and properties.

4.3. Experimental possibilities

Figure 4 presents the results of the subtraction of total C_{60} cross section from the total cross sections of the compound in two configurations $F^- - C_{60}^{+(2p)}$ and $F^- - C_{60}^{+(H)}$. The deviation of the results from the total cross section of free F^- ion (shown) captures the net effect of the atom-fullerene

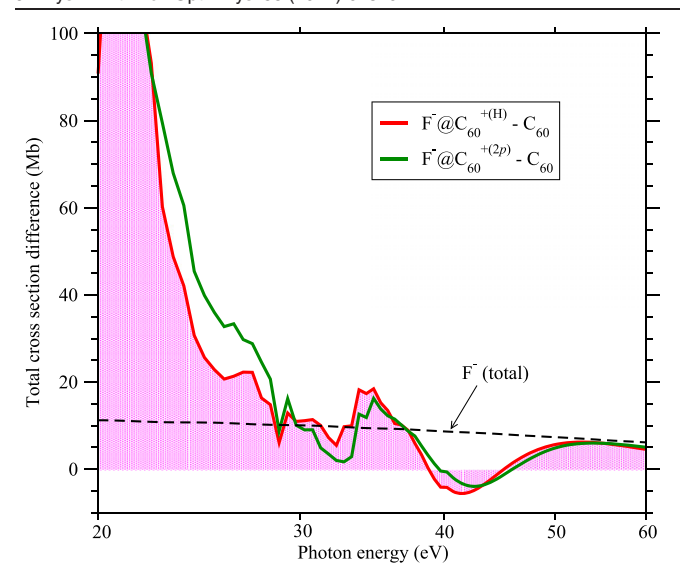


Figure 4. The magnitude differences of the total photoionization cross sections of $F^-@C_{60}^{+(H)}$ and $F^-@C_{60}^{+(2p)}$ from that of the empty C_{60} . Some smoothing is included. The total cross sections of F^- is presented for comparison.

coherence following the electron transfer. As is evident, constructive interferences from this coherence is seen near the C_{60} giant plasmon resonance energies. Surprisingly, however, this effect at the higher energy (weaker) plasmon resonance around 40 eV is found rather destructive; probing this can also be interesting given experimental abilities to observe this resonance [47]. Thus, such coherence effects can be directly probed by total photoionization cross section measurements by, for instance, the techniques utilized earlier based on detection and analysis of photoions [8-10]. In fact, such measurements can be extended for other halogen endofullerenes as well. Since the results in figure 4 also accounts for the differences between vacancy positions, the comparison with measurements may further shed light on the possible configuration of the molecule in its ground state. Figure 3 indicates that going up to 60 eV the calculated cross sections can drop as much as by three orders of magnitude which may pose challenges in measurements. However, the experimental signal will likely also include contributions from the atomic carbon ionization to augment the data with increasing energies [11]. Therefore, the cross section differences in figure 4 become particularly useful, since carbon contributions may largely cancel out to capture the effects of hybridization.

Another method to explore the situation experimentally is to use one laser pulse to excite $F@C_{60}$ by inducing an electron transfer and another pulse to ionize the hybrid levels to probe excited state cross sections. Such two-color two-step photoionization measurement techniques have been used earlier [48–50]. Based on this technique, an electron can be selectively promoted from a chosen C_{60} level, namely C_{60} HOMO or a hybrid level, to form metastable configurations. The comparison between spectra for photoelectrons driven by the subsequent second laser allows access to ionization properties as a function of the vacancy level.

Synthesis of halogen endofullerenes in vapor-phase has not been reported yet. But this may be possible by, for instance, halogen ion implantation techniques as adopted for other systems [51]. Perhaps because of the noncovalent interactions of these molecules with the environment their photoionization response will remain largely intact in some stable salt form, or in solutions or as thin films.

5. Conclusions

We previously studied [25, 26] the photoionization of various halogen-atomic (Cl, Br and I) endofullerene molecules with a C₆₀ electron relocated to the halogen atom likely forming metastable configurations. Those studies predicted that the effect of atom-C₆₀ hybridization on both ground state and photoemission properties is practically insensitive to the location of the vacancy level in C₆₀. In the current investigation we find a strong exception to this rule for such a metastable system F⁻@C₆₀⁺ made of the remaining halogen atom F. This exception reveals a novel effect based on the relative positions of the levels that hybridize in the compound. It is found that since, unlike to other halogens, the participating F level is more bound than the partner C₆₀ level, the increased screening due to the transfer of the electron results in a level crossing mechanism. Due to this mechanism, the degree of hybridization is significantly altered based on the vacancy creation in the hybrid-active versus a pure C₆₀ level. Consequently the hybrid photoemission properties become a very sensitive function of the vacancy position. The calculations are performed in a linear-response time-dependent density functional scheme, as was also employed in previous studies. We have discussed ideas for experiments to verify the predictions. Even though the effect is unique for $F^-@C_{60}^+$ for the halogen series, the precondition of such level-crossing effect can easily be satisfied for some of the other atoms, or small molecules, or metal cluster trapped in C₆₀ or even, in general, for different choices of the fullerenes itself, given that the atom-fullerene hybridization is a ubiquitous phenomenon in a host of these materials. In other words, we expect that this is a very general phenomenon and studies extended to the host of fullerene derivatives can uncover new spectroscopic effects possibly charting a new sub-field.

In our calculations, the C_{60} ion core is smeared in a jellium spherical shell that freezes lattice vibrations. Effectively, this mimics results at absolute zero sample temperature. However, it was shown earlier [32] that finite oven temperature effects, such as, the electron–phonon coupling [52] and fluctuation of the shape around the shape at absolute zero [53], approximately needed an extra width less than 1 eV to compare with measurements for C_{60} . This width is smaller than an energy resolution of about 5 eV required to measure broad structures in figures 3 and 4. Thus, while the thermal vibration will likely wash out the autoionizing spikes, it would not qualitatively alter the key results of this study. Furthermore, possible temperature driven oscillations [54] of the confined atom may broaden and lower some narrow structures in the signal, but most of the features in the current results

being broad enough will survive. As an example, the measurement of the confinement induced structures in $Xe@C_{60}$ was possible in the laboratory at a temperature well above absolute zero [9, 10]. Of course, the colder the sample temperature, the closer to the predictions the measurements can come. Besides encouraging experiments, the other aim of the study is to motivate simulations including fullerene lattice vibration and phonon coupling effects. However, this will be rather challenging. Because, while the molecular structure can readily be improved by employing sophisticated methods to include lattice vibrations, the photoionization will require calculations of continuum wavefunctions including electron correlation in the electron–phonon coupled frame.

Acknowledgments

The research is supported by the US National Science Foundation Grant Nos. PHY-1806206 (HSC) and PHY-2135107 (HSC), and the US Department of Energy, Office of Science, Basic Energy Sciences, under Award DE-FG02-03ER15428 (STM).

Data availability statement

All data that support the findings of this study are included within the article (and any supplementary files).

ORCID iDs

Esam Ali https://orcid.org/0000-0002-4836-8520 Mohamed El-Amine Madjet https://orcid.org/0000-0002-8910-2278

Steven T Manson https://orcid.org/0000-0002-7072-4122 Himadri S Chakraborty https://orcid.org/0000-0001-5758-6418

References

- Popov A A 2017 Synthesis and molecular structures of endohedral fullerenes Endohedral Fullerenes: Electron Transfer and Spin (Nanostructure Science and Technology Series) ed A A Popov (Berlin: Springer)
- [2] Ross R B et al 2009 Endohedral fullerenes for organic photovoltaic devices Nat. Mater. 8 208
- [3] Takeda A et al 2006 Superconductivity of doped Ar@C₆₀ Chem. Commun. 8 912
- [4] Harneit W, Boehme C, Schaefer S, Huebener K, Fostiropoulos K and Lips K 2007 Room temperature electrical detection of spin coherence in C₆₀ Phys. Rev. Lett. 98 216601
- [5] Ju C, Suter D and Du J 2011 An endohedral fullerene-based nuclear spin quantum computer Phys. Lett. A 375 1441
- [6] Chandler H J, Stefanou M, Campbell E E B and Schaub R 2019 Li@C₆₀ as a multi-state molecular switch *Nat. Commun.* 10 2283
- [7] Melanko J B, Pearce M E and Salem A K 2009 Nanotechnology in Drug Delivery ed M M de Villiers, P Aramwit and G S Kwon (New York: Springer) p 105

- [8] Müller A, Schippers S, Habibi M, Esteves D, Wang J C, Phaneuf R A, Kilcoyne A L D, Aguilar A and Dunsch L 2008 Significant redistribution of Ce 4d oscillator strength observed in photoionization of endohedral Ce@C₈₂⁺ ions Phys. Rev. Lett. 101 133001
- [9] Kilcoyne A L D et al 2010 Confinement resonances in photoionization of Xe@C₆₀⁺ Phys. Rev. Lett. 105 213001
- [10] Phaneuf R A et al 2013 Probing confinement resonances by photoionizing Xe inside a ${\rm C_{60}}^+$ molecular cage Phys. Rev. A 88 053402
- [11] Rüdel A, Hentges R, Becker U, Chakraborty H S, Madjet M E and Rost J M 2002 Imaging delocalized electron clouds: photoionization of C₆₀ in fourier reciprocal space *Phys. Rev. Lett.* 89 125503
- [12] Dolmatov V K 2009 Photoionization of atoms encaged in spherical fullerenes, theory of confined quantum systems: II Advances in Quantum Chemistry vol 58 ed J R Sabin and E Braendas (New York: Academic) pp 13–68
- [13] Chakraborty H S and Magrakvelidze M 2015 Many-electron response of gas-phase fullerene materials to ultraviolet and soft x-ray photons From Atomic to Mesoscale: The Role of Quantum Coherence in Systems of Various Complexities ed S Malinovskaya and I Novikova (Singapore: World Scientific) p 221
- [14] Chakraborty H S, Madjet M E, Renger T, Rost J-M and Manson S T 2009 Photoionization of hybrid states in endohedral fullerenes *Phys. Rev.* A 79 061201(R)
- [15] Madjet M E, Renger T, Hopper D E, McCune M A, Chakraborty H S, Rost J-M and Manson S T 2010 Photoionization of Xe inside C₆₀: atom-fullerene hybridization, giant cross-section enhancement, and correlation confinement resonances *Phys.* Rev. A 81 013202
- [16] Maser J N, Javani M H, De R, Madjet M E, Chakraborty H S and Manson S T 2012 Atom-fullerene hybrid photoionization mediated by coupled d states in Zn@C₆₀ Phys. Rev. A 86 053201
- [17] Javani M H, De R, Madjet M E, Manson S T and Chakraborty H S 2014 Photoionization of bonding and antibonding-type atom-fullerene hybrid states in Cd@C₆₀ vs Zn@C₆₀ J. Phys. B: At. Mol. Opt. Phys. 47 175102
- [18] Javani M H, Wise J B, De R, Madjet M E, Manson S T and Chakraborty H S 2014 Resonant Auger-intercoulombic hybridized decay in the photoionization of endohedral fullerenes *Phys. Rev.* A 89 063420
- [19] Lawler R G 2017 Nonmetallic endofullerenes and the endohedral environment: structure, dynamics, and spin chemistry Endohedral Fullerenes: Electron Transfer and Spin ed A Popov (Berlin: Springer) p 229
- [20] Morton J J L, Tyryshkin A M, Ardavan A, Porfyrakis K, Lyon S A and Briggs G A D 2007 Environmental effects on electron spin relaxation in N@C₆₀ Phys. Rev. B 76 085418
- [21] Knapp C, Weiden N, Kass H, Dinse K-P, Pietzak B, Waiblinger M and Weidinger A 1998 Electron paramagnetic resonance study of atomic phosphorus encapsulated in [60] fullerene Mol. Phys. 95 999
- [22] Donzelli O, Briere T and Das T P 1996 Location of muonium and hydrogen in C₆₀ fullerene and associated electronic structure and hyperfine properties *Hyperfine Interact*. 97–98
- [23] Ma F, Li Z-R, Zhou Z-J, Wu D, Li Y, Wang Y-F and Li Z-S 2010 Modulated nonlinear optical responses and charge transfer transition in endohedral fullerene dimers Na@C₆₀C₆₀@F with *n*-fold covalent bond (n = 1, 2, 5, and 6) and long range ion bond *J. Phys. Chem* C 114 11242
- [24] Foroutan-Nejad C, Straka M, Fernández I and Frenking G 2018 Buckyball difluoride F₂⁻@C₆₀⁺ a single-molecule crystal Angew. Chem., Int. Ed. 57 13931
- [25] Shields D, De R, Madjet M E, Manson S T and Chakraborty H S 2020 Photoemission from hybrid states of Cl@C₆₀ before

- and after a stabilizing charge transfer *J. Phys. B: At. Mol. Opt. Phys.* **53** 125101
- [26] Shields D, De R, Ali E, Madjet M E, Manson S T and Chakraborty H S 2020 A density functional theory based comparative study of hybrid photoemissions from Cl@C₆0, Br@C₆₀ and I@C₆₀ Eur. Phys. J. D 74 191
- [27] Felfli Z, Suggs K, Nicholas N and Msezane A Z 2020 Fullerene negative ions: formation and catalysis Int. J. Mol. Sci. 21 3159
- [28] Chakraborty H S, Gray A, Costello J T, Deshmukh P C, Haque G N, Kennedy E T, Manson S T and Mosnier J-P 1999 Anomalous behavior of the near-threshold photoionization cross section of the neon isoelectronic sequence: a combined experimental and theoretical study *Phys. Rev. Lett.* 83 2151
- [29] Oh S, Huang Z, Peskin U and Kais S 2008 Entanglement, Berry phases, and level crossings for the atomic Breit–Rabi Hamiltonian *Phys. Rev.* A 78 062106
- [30] Glenn R and Dantus M 2016 Molecular level crossing and the geometric phase effect from the optical Hanle perspective *Phys. Rev.* A 93 043402
- [31] Lang F, Straten P v d., Brandstätter B, Thalhammer G, Winkler K, Julienne P S, Grimm R and Hecker Denschlag J 2008 Cruising through molecular bound-state manifolds with radiofrequency *Nat. Phys.* 4 223
- [32] Madjet M É, Chakraborty H S, Rost J M and Manson S T 2008 Photoionization of C₆₀: a model study J. Phys. B: At. Mol. Opt. Phys. 41 105101
- [33] Van Leeuwen R and Baerends E J 1994 Exchange-correlation potential with correct asymptotic behavior *Phys. Rev.* A 49 2421
- [34] Choi J, Chang E H, Anstine D M, Madjet M E and Chakraborty H S 2017 Effects of exchange-correlation potentials on the density-functional description of C₆₀ versus C₂₄₀ Phys. Rev. A 95 023404
- [35] Ravinder P and Subramanian V 2011 Studies on the encapsulation of various anions in different fullerenes using density functional theory calculations and Born–Oppenheimer molecular dynamics simulation J. Phys. Chem A 115 11723
- [36] Baltenkov A S, Dolmatov V K, Manson S T, Msezane A Z and Pikhut V A 2003 Trends in near-threshold photoionization of off-the-center endohedral atoms *Phys. Rev.* A 68 043202
- [37] Dolmatov V K and Manson S T 2010 Interior static polarization effect in A@C₆₀ photoionization *Phys. Rev.* A 82 023422
- [38] de Vries J, Steger H, Kamke B, Menzel C, Weisser B, Kamke W and Hertel I V 1992 Single-photon ionization of C₆₀- and C₇₀-fullerene with synchrotron radiation: determination of the ionization potential of C₆₀ Chem. Phys. Lett. 188 159
- [39] Magrakvelidze M, Anstyne D M, Dixit G, Madjet M E and Chakraborty H S 2015 Attosecond structures from

- molecular cavity in fullerene photoemission time delay *Phys. Rev.* A **91** 053407
- [40] Lu J, Zhang X and Zhao X 1999 Electronic structures of endohedral N@C60, O@C60 and F@C60 Chem. Phys. Lett. 312 85
- [41] Manz T A and Limas N G 2016 Introducing DDEC6 atomic population analysis: I. Charge partitioning theory and methodology RSC Adv. 6 47771
- [42] De R, Magrakvelidze M, Madjet M E, Manson S T and Chakraborty H S 2016 First prediction of inter-Coulombic decay of C₆₀ inner vacancies through the continuum of confined atoms J. Phys. B: At. Mol. Opt. Phys. 49 11LT01
- [43] Madjet M E, Chakraborty H S and Manson S T 2007 Giant enhancement in low energy photoemission of Ar confined in C₆₀ Phys. Rev. Lett. 99 243003
- [44] Fano U 1961 Effects of configuration interaction on intensities and phase shifts *Phys. Rev.* **124** 1866
- [45] Connerade J P, Dolmatov V K and Manson S T 2000 On the nature and origin of confinement resonances J. Phys. B: At. Mol. Opt. Phys. 33 2279
- [46] McCune M A, Madjet M E and Chakraborty H S 2009 Reflective and collateral photoionization of an atom inside a fullerene: confinement geometry from reciprocal spectra *Phys. Rev.* A 80 011201(R)
- [47] Scully S W J et al 2005 Photoexcitation of a volume plasmon in C₆₀ Ions Phys. Rev. Lett. 94 065503
- [48] Zheng X, Zhou X, Cheng Z, Jia D, Qu Z, Yao G, Zhang X and Cui Z 2014 Photoionization cross section measurements of the excited states of cobalt in the near-threshold region AIP Adv. 4 107120
- [49] Yar A, Ali R and Baig M A 2013 Evidence of a Cooper minimum in the photoionization from the $7s^2S_{1/2}$ excited state of potassium *Phys. Rev.* A **88** 033405
- [50] Sell J F, Patterson B M, Ehrenreich T, Brooke G, Scoville J and Knize R J 2011 Lifetime measurement of the cesium ⁶P_{3/2} state using ultrafast laser-pulse excitation and ionization *Phys. Rev.* A 84 010501(R)
- [51] Campbell E E B, Tellgmann R, Krawez N and Hertel I V 1997 Production and LDMS characterisation of endohedral alkalifullerene films J. Phys. Chem. Solids 58 1763
- [52] Bertsch G F and Tománek D 1989 Thermal line broadening in small metal clusters *Phys. Rev.* B 40 2749
- [53] Pacheco J M and Broglia R A 1989 Effect of surface fluctuations in the line shape of plasma resonances in small metal clusters *Phys. Rev. Lett.* 62 1400
- [54] Korol A V and Solov'yov A V 2010 Confinement resonances in the photoionization of endohedral atoms: myth or reality? J. Phys. B: At. Mol. Opt. Phys. 43 201004